Published in "Journal of Chemical Physics 124: 024511, 2006"
which should be cited to refer to this work.

Cs^*He_n exciplexes in solid ^4He

P. Moroshkin,* A. Hofer, D. Nettels, S. Ulzega, and A. Weis
Département de Physique, Université de Fribourg,
Chemin du Musée 3, 1700 Fribourg, Switzerland†
(Dated: June 22, 2006)

We present a theoretical and experimental study of the laser-induced formation process and of the emission spectra of Cs^*He_n exciplexes in the hcp and bcc phases of solid helium. Two different exciplex molecules are detected: a linear triatomic Cs^*He_2, which can exist in two electronic states: $A\Pi_{1/2}$ and $B\Pi_{3/2}$, and a larger complex, where 6 or 7 He atoms form a ring around a single cesium atom in the $6P_{1/2}$ state. A theoretical model is presented, which allows the interpretation of the experimentally observed spectra.

I. INTRODUCTION

Alkali atoms and helium atoms in their ground states strongly repel each other at small internuclear distances, however, an alkali atom excited to one of its P states can exert an attractive force on nearby helium atoms, and form bound states, known as exciplexes. The formation of alkali-helium exciplexes was considered for the first time by Dupont-Roc [1] and Kanorsky et al. [2] as an explanation for the observed quenching of atomic fluorescence from light alkali atoms (Na, Li) embedded in liquid and solid ^4He. In the meantime such exciplex molecules have been observed in liquid helium and in cold helium gas [3–5], as well as on the surface of helium nanodroplets [6–9]. In this paper we present a theoretical and experimental study of cesium-helium exciplexes formed in a solid helium matrix, and give a more detail account on our recent observation [10] of these complexes.

The alkali valence electron repels helium atoms because of the Pauli principle. However, when a helium atom approaches the alkali atom along a nodal line or a nodal plane of the latter's electron density distribution, it experiences an attractive van der Waals force until it is repelled by the alkali core. The spin-orbit interaction splits the lowest excited state of an alkali atom into $P_{3/2}$ and $P_{1/2}$ fine-structure components. The $m_j = \pm 3/2$ sublevels of the former have an apple-shaped electron density distribution, and can bind up to two helium atoms along their nodal axis, in a diatomic, or a linear triatomic configuration. The $P_{1/2}$ orbital is spherically symmetric, but may loose this symmetry if the interaction with helium becomes comparable to, or stronger than the spin-orbit coupling in the alkali atom. In this case the valence electron distribution becomes dumbbell-shaped, similar to a spin-orbit uncoupled P_z orbital and can accommodate several helium atoms. Dumbbell-shaped exciplexes with more than 2 helium atoms have been observed for Na [5], K [5, 6], and Rb [4], for which the alkali-helium interaction dominates over the spin-orbit interaction. Cesium has a particular behavior because it has the strongest spin-orbit coupling of all the (stable) alkali elements. Therefore exciplexes with more than 2 helium atoms can only be observed in a He surrounding of very high density, such as solid He [10].

A detailed comparative analysis of $Cs^*He_{n=1,2}$ and $Rb^*He_{n=1...6}$ exciplexes was performed by the Kyoto group [3, 4]. The authors have considered the formation of the exciplexes as a sequential process, in which helium atoms are attached to the complex one by one. It was found that for rubidium all exciplexes with n=3-6 have a total energy below the dissociation limit, and are therefore stable. For cesium, however, the exciplex with three helium atoms is unstable and therefore its formation and hence the subsequent formation of larger exciplexes was expected to be suppressed. Experiments in cold helium gas, in which the relatively low collision rate justifies an analysis in terms of sequential capture processes, have indeed shown [3] that only Cs^*He_1 and Cs^*He_2 exciplexes are formed, with no evidence for complexes with $n > 2$.

In our recent publication [10] we have reported the observation of several new spectral lines in the laser-induced fluorescence spectra of cesium atoms embedded in solid helium. The emission lines were strongly red shifted with respect to the atomic fluorescence line. We have attributed those lines to fluorescence from Cs^*He_n exciplexes. Based on our theoretical modelling of the exciplex potentials and the corresponding fluorescence lines [10] we have demonstrated unambiguously that Cs^*He_n exciplexes with $n > 2$ are formed, when cesium atoms embedded in solid helium are excited to the $6P_{3/2}$ state. From a comparison of integrated line intensities we have concluded that the formation of those exciplexes is the most probable deexcitation channel of the $6P_{3/2}$ state.

Here we present further experimental and theoretical details of the structure and emission spectra of Cs^*He_n exciplexes. The article is organized as follows: in Sec. II we present the theoretical model of the exciplex structure, Sec. III describes the experiments and their results, in Sec. IV the formation mechanisms of different exciplexes are discussed. The main results are summarized

*peter.moroshkin@unifr.ch
†www.unifr.ch/physics/frap/

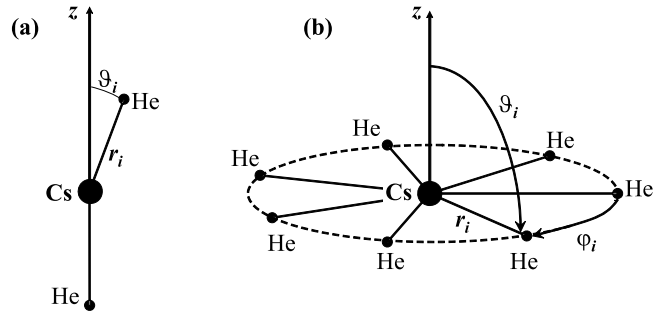

FIG. 1: Structure of Cs^*He_n exciplexes: (a) Linear Cs^*He_2 molecule. The position vector of the i-th helium atom is: $\mathbf{r}_i = \mathbf{r}(r, \theta_i = \pi(i-1), \varphi)$. (b) $Cs^*He_{n>2}$ complex with $\mathbf{r}_i = \mathbf{r}(r, \theta = \pi/2, \varphi_i = i2\pi/n)$.

in Sec. V.

II. THEORETICAL MODEL

Our modelling of the structure and emission spectra of Cs^*He_n exciplexes follows the approach of [3, 4].

As the emission spectra are mainly determined by the n bound helium atoms we consider only the influence of those atoms and neglect the influence of the bulk of the surrounding helium matrix. The validity of this approach will be addressed in Sec. III D.

A. Cs^*-He_n exciplex potentials

The interaction between one cesium atom and n He atoms is described as a sum over adiabatic molecular two-body interaction potentials. We use the potentials between a helium ground state atom and an alkali atom in its ground and lower excited states calculated by Pascale [11]. For the 6S ground state the potential, denoted by $V_\sigma^{6s}(r)$, is radially symmetric. For the 6P states the interaction is anisotropic and can be expressed by the operator

$$V^{6P}(\mathbf{r}) = V_\sigma^{6P}(r) + \left(\frac{\mathbf{L}\cdot\mathbf{r}}{\hbar r}\right)^2 [V_\pi^{6P}(r) - V_\sigma^{6P}(r)], \quad (1)$$

where $\mathbf{r} = \mathbf{r}(r, \theta, \varphi)$ denotes the position vector of a helium atom with respect to the cesium atom and $\mathbf{L}$ is the electronic angular momentum operator of the cesium atom [1]. Stable exciplexes of the form $Cs^*He_{n=2}$ are formed by two helium atoms located on a common axis on opposite sides of the cesium atom. For $Cs^*He_{n\geq 3}$ we consider only a configuration where the helium atoms are distributed on a concentric ring around the alkali atom. These structures are represented in Fig. 1, where we introduce spherical coordinate systems with the origin at the position of Cs atom. The summation over the pair potentials can be expressed by the operator (for $n = 1, 2, ...n_{max}$)

$$V_n^{Cs\text{-}He}(r) = \sum_{i=1}^{n} V^{6P}(\mathbf{r}_i), \quad (2)$$

with $\mathbf{r}_i = \mathbf{r}(r, \theta_i = \pi(i-1), \varphi)$ for $n = 1, 2$, and $\mathbf{r}_i = \mathbf{r}(r, \theta = \pi/2, \varphi_i = i2\pi/n)$ for $n \geq 3$, where we have chosen the same value of r for all involved He atoms. In addition we include He-He interactions by summing over the corresponding potentials $V_{He\text{-}He}(|\mathbf{r}_i - \mathbf{r}_{i+1}|)$ between neighboring helium atoms. The He-He interaction is modelled by the *ab initio* potential given by Aziz [12]. The distance between two neighboring helium atoms is a function of the cesium-helium separation r and the number n of helium atoms with $|\mathbf{r}_i - \mathbf{r}_{i+1}| = 2r\sin(\pi/n)$. The summation over all helium pairs then gives

$$V_n^{He\text{-}He}(r) = nV_{He\text{-}He}(2r\sin(\pi/n)) \quad (3)$$

After including the spin-orbit interaction in the cesium atom the total interaction potential of the Cs^*He_n system reads

$$V_{Cs^*He_n}(r) = V_n^{Cs\text{-}He}(r) + V_n^{He\text{-}He}(r) + 2/3\Delta\mathbf{L}\cdot\mathbf{S}, \quad (4)$$

where Δ is the fine-structure splitting of the cesium 6P state and $\mathbf{S}$ is the electronic spin operator. As we ignore here any influence of the He matrix, we use the value

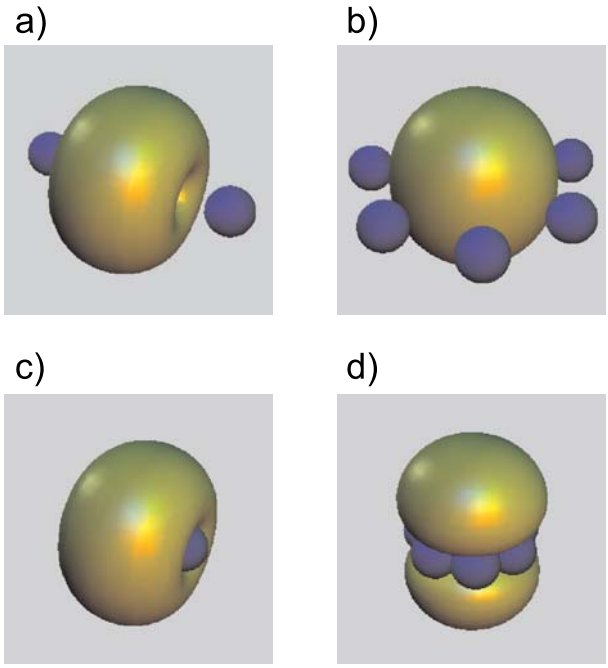

FIG. 2: Calculated electron density distribution of $Cs(B\Pi_{3/2})He_2$ (a, c) and $Cs(A\Pi_{1/2})He_7$ (b, d) complexes. (a) and (b) represent an initial stage of the exciplex formation with $r = 6.5$ Å, that corresponds to the radius of a He bubble. (c) and (d) show the exciplex structures in their equilibrium configuration at $r = 3.5$ Å.

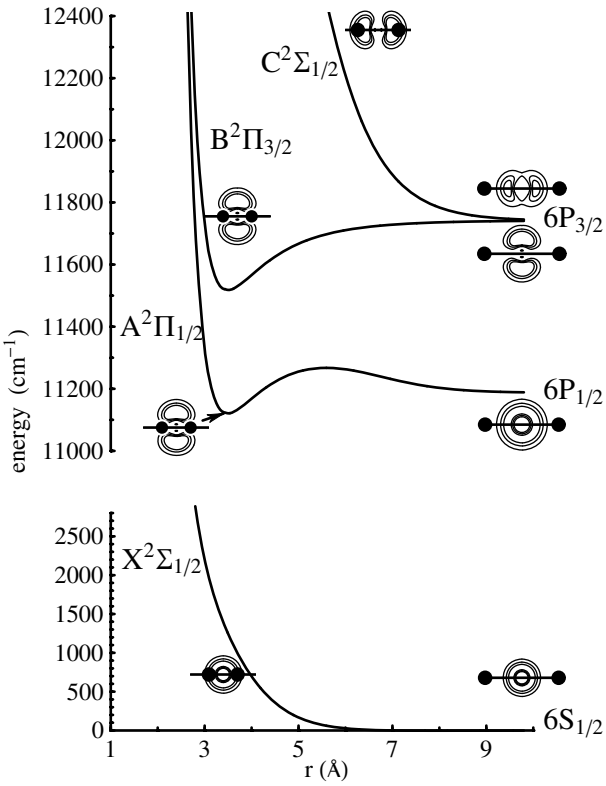

FIG. 3: Adiabatic potentials of the Cs*He$_2$ system, including the spin-orbit interaction. The two helium atoms are located at $z = r$ and $z = -r$ on the quantization (rotational symmetry) axis, indicated in the pictographs by a solid line. The shape of the electronic density distribution of the cesium atom changes significantly as helium atoms (filled circles) approach.

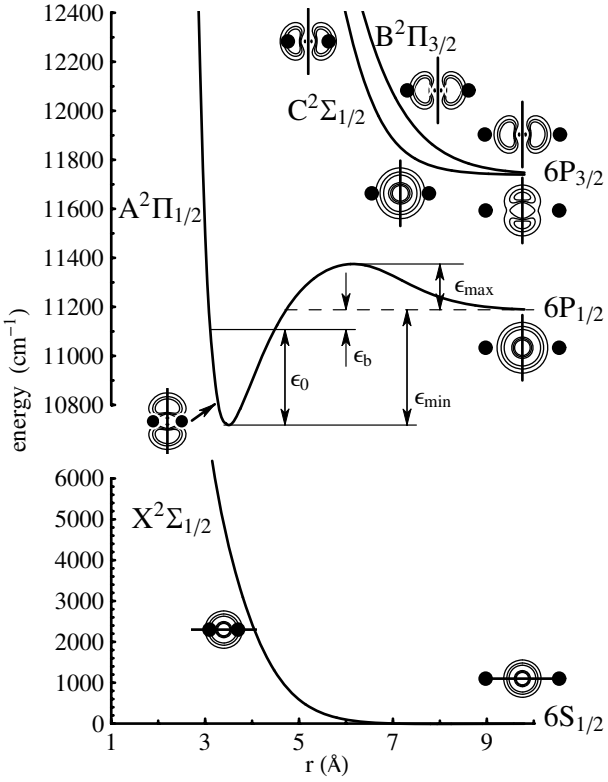

FIG. 4: Adiabatic potentials of the Cs*He$_7$ system. The seven helium atoms are located on a ring of radius r concentric with the symmetry axis. ϵ_{min}, ϵ_{max}, ϵ_0, and ϵ_b represent the depth of the potential well, the height of the potential barrier, the energy of the vibrational ground state, and its binding energy, all with respect to the asymptotic energy of the free atomic $P_{1/2}$ state.

$\Delta = 554.0$ cm^{-1} of the free Cs atom. As a last step, $V_{Cs^*He_n}(r)$ is diagonalized algebraically.

In Figs. 3 and 4 the resulting r-dependence of the eigenvalues are shown for Cs*He$_2$ and Cs*He$_7$ respectively. The same plots also show the ground state potentials given by

$$nV_\sigma^{6s}(r) + V_n^{He\text{-}He}(r) \qquad (5)$$

The quantization axis is defined by the symmetry axis of the exciplexes, which is the internuclear axis of the cesium atom and the two helium atoms in the case of Cs*He$_{n=1,2}$, whereas for Cs*He$_{n\geq 3}$ it is the axis of the helium ring. Although the standard spectroscopic notations $X^2\Sigma_{1/2}$, $A^2\Pi_{1/2}$, $B^2\Pi_{3/2}$ and $C^2\Sigma_{1/2}$ apply only for linear molecules, we retain the same notation for simplicity to label all exciplexes.

From the adiabatic potentials of Fig. 3 one sees that when two helium atoms approach along a nodal line of an apple-shaped electron distribution ($B^2\Pi_{3/2}$ configuration) they experience an attractive van der Waals force, which results in the formation of Cs($B\Pi_{3/2}$)He$_2$ molecules, that were studied in [3] and [10].

Two helium atoms can also be bound in a $A^2\Pi_{1/2}$ configuration. The situation is more complicated as the spherically symmetric 6P$_{1/2}$ state is repulsive at large distances. However, when one, or two helium atoms approach it sufficiently, the electronic wave function looses its spherical character and becomes apple-shaped, similar to the 6P$_{3/2}$ state. Helium atoms are then attracted by the van der Waals force along its nodal line and may form an exciplex. The potential barrier of the $A^2\Pi_{1/2}$ state at $r = 6.5$ Å is associated with this deformation.

For Cs*He$_{n\geq 3}$, there are no attractive minima in the potential curves originating from the 6P$_{3/2}$ state of the cesium atom (Fig. 4). However, in a similar way as discussed above, the electronic wave function of the spherical 6P$_{1/2}$ state may be deformed by the interaction with helium. If more than two helium atoms are in close proximity, the spherical 6P$_{1/2}$ state becomes dumbbell-shaped. Once the helium atoms have overcome the barrier in the $A^2\Pi_{1/2}$ configuration (Fig. 4) they will be attracted along the nodal plane and will form an exciplex with $n > 2$. Emission lines of such exciplexes are further red-shifted with respect to Cs($B\Pi_{3/2}$)He$_2$ and were observed for the first time in [10].

The electronic densities of the Cs($B\Pi_{3/2}$)He$_2$ and Cs($A\Pi_{1/2}$)He$_7$ complexes are illustrated in Fig. 2 for the

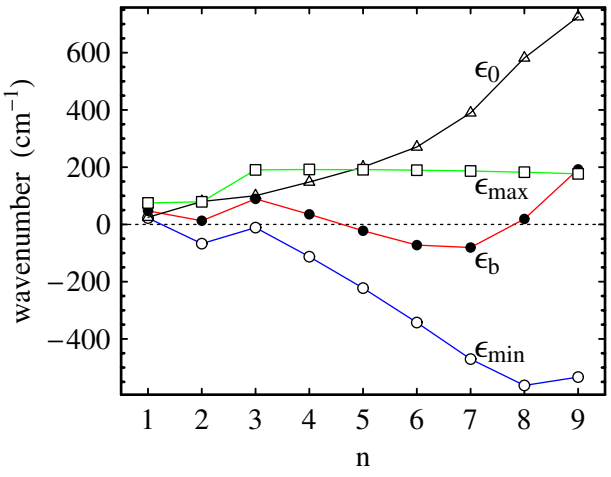

FIG. 5: Energy dependencies of the Cs($A^2\Pi_{1/2}$)He_n exciplexes as a function of the number n of helium atoms. Shown are the minimal energies $\epsilon_{min}^{(n)}$ (open circles) of the potential wells, the barrier heights $\epsilon_{max}^{(n)}$ (open squares), the total zero-point energies $\epsilon_0^{(n)}$ (triangles), and the binding energies $\epsilon_b^{(n)}$ (filled circles). All energies are given with respect to the dissociation limit, i.e., the electronic energy of the $6P_{1/2}$ state. Corresponding points are joined by lines to guide the eye.

interatomic distances of $r = 6.5$ and 3.5 Å. The former correspond to the relative positions of Cs and He atoms at the onset of the exciplex formation process as discussed in Sec. IV, while the latter correspond to the equilibrium configuration. The transformations of the density distribution of the valence electron of cesium atom are also illustrated by the pictographs shown as inserts in Figs. 3 and 4. In these pictographs, the electronic density of cesium is represented by cuts through the electron orbitals. For calculating the equi-density lines we used radial wavefunctions of the cesium 6S and 6P states obtained from the Schrödinger equation with a statistical Thomas-Fermi model of the atom following a procedure given by Gombas [13]. The angular parts of the wavefunctions are the eigenvectors of $V_{Cs^*He_n}(r)$ expressed as a linear combinations of the $|J, m_j\rangle$ states of the Cs atom. The helium atoms are shown as spheres with a diameter of 3.5 Å, which corresponds to the mean interatomic distance in the helium bulk.

We have calculated the adiabatic potentials for all Cs^*He_n systems up to $n = 9$. The n dependence of the potential well depths $\epsilon_{min}^{(n)}$ of the $A\Pi_{1/2}$ electronic states is represented in Fig. 5 by open circles. The values are given with respect to the dissociation limit, i.e., the energy of the $6P_{1/2}$ state of the free cesium atom. For $n > 3$ the energy drops with increasing n. However as the distance between neighboring helium atoms becomes smaller their interatomic repulsion exceeds the attractive cesium-helium interaction. The configuration with $n = 8$ has the deepest attractive potential. Also shown in Fig. 5 (open squares) are the heights of the potential barriers as a function of n. The barrier increases significantly when going from Cs^*He_2 to Cs^*He_3 above which it reaches an almost constant value. This reflects the fact discussed above that the binding of a third helium atom is accompanied by a significant change of the electronic configuration from apple-shaped to dumbbell-shaped.

B. Ro-vibrational structure of the Cs^*He_n exciplexes

In order to investigate the stability of the exciplexes, one has to calculate the total energies of the bound states by including contributions from the vibrational motion of the helium atoms in the exciplex molecule. The rotational energies of the exciplex (for rotations around the symmetry axis) are given by

$$\epsilon_k = k(k+1)\frac{\hbar^2}{2I}, \tag{6}$$

where I is the momentum of inertia of the molecule. For the equilibrium configurations of the considered complexes the rotational quanta are of the order of 0.1 cm^{-1}, hence at the temperature of 1.5 K several excited rotational states are populated. This rotational structure can not be resolved in our experiments and we neglect it in the following discussion.

First, we analyze the structure of normal vibrational modes using a standard procedure [**?**] assuming that the total potential energy of the molecule is represented as a sum over (Cs-He and He-He) pair potentials. An exciplex formed by a cesium atom and n helium atoms has $3(n+1)$ degrees of freedom. After removing three degrees of freedom for the center of mass position, two degrees of freedom for the spatial orientation of the symmetry axis and one degree of freedom for the collective rotation around the symmetry axis of the exciplex one is left with $3(n-1)$ vibrational degrees of freedom. The corresponding vibrational modes consist of n radial modes (r-modes), $n-2$ polar modes (θ-modes) and $n-1$ azimuthal modes (φ-modes), where θ and φ are spherical coordinates with respect to the exciplex axis. This decomposition makes only sense for $n \geq 3$ as the diatomic Cs^*He_1 molecule has only a single radial mode. The linear triatomic Cs^*He_2 molecule has two stretching modes and two bending modes.

The vibrational energies of a given mode of type α involving n helium atoms are given by

$$\epsilon_{N_\alpha}^{(n)} = \epsilon_\alpha^{(n)}(2N_\alpha + 1), \tag{7}$$

where N_α and $\epsilon_\alpha^{(n)}$ are the corresponding vibrational quantum numbers and zero point energies.

Up to $n = 6$ the strongest force on the bound He atoms is in the radial direction, so that the energies of the radial modes are much larger than those of θ- and φ-modes. Because of the non-spherical symmetry of the potential the vibrational eigenmodes will be combinations of the $r-, \theta$-

and φ-modes. However, the φ-modes are decoupled from the $r-, \theta$-modes as they are determined by He-He interaction only. In order to simplify the the analysis we assume the θ- modes also to be decoupled. It is reasonable to assume that the energies of the different modes within each subgroup (r-, θ-, φ-modes) are nearly degenerate, so that we can restrict the discussion to a single representative mode for each group.

For the group of radial vibrations we consider the symmetric (breathing) mode, in which all helium atoms make a collective oscillation in the radial direction. We have solved the corresponding one-dimensional Schrödinger equation numerically for each Cs^*He_n molecule (n = 1...9). The energies of the lowest vibrational states are separated by about 50-60 cm^{-1}, which corresponds to 70-90 K, so that in thermal equilibrium at the temperature of the experiments (1.5 K) the higher vibrational states are not populated and can be neglected. Under the assumption that all other radial modes are degenerate with the breathing mode the total energy of the radial oscillations is given by $\epsilon_r^{(n,\ tot)} = n\epsilon_r^{(n)}$, where $\epsilon_r^{(n)}$ is the zero point energy of the breathing mode, whose wave function is $\Psi_{sym}(r)$.

From the group of polar oscillations we treat only the symmetric mode parameterized by

$$\mathbf{r}_i = \mathbf{r}(r_0, \theta = \pi/2 + \delta\theta, \varphi_i = i2\pi/n) \tag{8}$$

where $\delta\theta$ is the oscillation angle and r_0 the equilibrium radius of the He ring. The zero point energy $\epsilon_\theta^{(n)}$ was found by solving the corresponding one-dimensional Schrödinger equation with the potential energy operator:

$$V_n^{Cs\text{-}He}(\delta\theta) = nV^{6P}(r_0, \delta\theta, \varphi = 0) \tag{9}$$

Assuming again that all polar oscillations are degenerate the total polar vibrational energy is given by $\epsilon_\theta^{(n,\ tot)} = (n-2)\epsilon_\theta^{(n)}$.

We estimate the energy spectrum of the azimuthal modes by considering only the mode, in which $n-1$ helium atoms are at rest at their equilibrium positions, while a single helium atom is allowed to oscillate between its two neighbors on the ring. The potential energy of this oscillation reads

$$\begin{aligned} V_n^{He\text{-}He}(\delta\varphi) \ &= \ V_{He\text{-}He}(2r_0 \sin(\pi/n + \delta\varphi)) \\ &\quad + V_{He\text{-}He}(2r_0 \sin(\pi/n - \delta\varphi)), \end{aligned}$$

where $\delta\varphi$ denotes the oscillation angle. The total zero point energy resulting from the corresponding Schrödinger equation is then approximately $\epsilon_\varphi^{(n,\ tot)} = (n-1)\epsilon_\varphi^{(n)}$.

The overall zero-point energy taking all vibrational modes into account is finally given by

$$\epsilon_0^{(n)} = \epsilon_r^{(n,\ tot)} + \epsilon_\varphi^{(n,\ tot)} + \epsilon_\theta^{(n,\ tot)}. \tag{10}$$

The contributions of radial, polar, and azimuthal vibrations to the total zero-point energy, as well as numerical values of $\epsilon_r^{(n)}$, $\epsilon_\theta^{(n)}$, and $\epsilon_\varphi^{(n)}$ for n = 1...9 are given in Table II B. The n dependence of $\epsilon_0^{(n)}$ is represented in Fig. 5 by triangles. We define the binding energy $\epsilon_b^{(n)}$ of the complex including one cesium atom and n helium atoms as the difference between its total energy and the dissociation limit:

n	$\epsilon_r^{(n)}$	$\varepsilon_\varphi^{(n)}$	$\varepsilon_\vartheta^{(n)}$	$\varepsilon_r^{(n,\ tot)}$	$\varepsilon_\varphi^{(n,\ tot)}$	$\varepsilon_\vartheta^{(n,\ tot)}$	$\epsilon_0^{(n)}$
1	25.0	0	0	25.0	0	0	25.0
2	26.8	0	13.2	53.7	0	26.4	80.1
3	27.1	0.1	19.1	81.3	0.2	19.1	100.6
4	27.3	1.8	19.3	109.4	5.1	38.7	153.2
5	27.5	1.2	19.4	137.3	4.7	58.3	200.3
6	27.6	5.3	19.5	165.7	26.7	78.1	270.5
7	28.5	15.4	19.5	199.5	92.7	97.6	389.8
8	30.2	32.1	19.2	241.7	224.4	115.5	581.6
9	25.2	46.5	18.2	226.5	371.6	127.4	725.5

TABLE I: Numerical values of the calculated vibration energies of $Cs(A\Pi_{1/2})He_{n=1...9}$ exciplexes (in cm^{-1}).

$$\epsilon_b^{(n)} = \epsilon_{min}^{(n)} + \epsilon_0^{(n)}. \tag{11}$$

Note that $\epsilon_{min}^{(n)}$ is measured with respect to the asymptotic energy of the free atomic $P_{1/2}$ state. Negative values of $\epsilon_b^{(n)}$ correspond to a total energy below the dissociation limit. The binding energy is represented in Fig. 5 by filled circles and has a local minimum for $n = 2$. After the strong increase between $n = 2$ and $n = 3$ it drops monotonically until it reaches a global minimum for $n = 7$. For larger n the zero point energy of the azimuthal modes increases rapidly due to the very tight confinement of the He atoms in the ring structure and $\epsilon_b^{(n)}$ becomes positive.

The calculations indicate that exciplexes with $n \geq 9$, for which the estimated total zero-point energy exceeds the barrier energy, are unstable (Fig. 5). $Cs(A\Pi_{1/2})He_8$ seems to be the largest possible quasi-bound exciplex. There are 3 possible stable exciplexes $Cs(A\Pi_{1/2})He_{5,6,7}$ with a zero-point energy well below the dissociation limit. The bound state with $n = 7$ has the lowest zero-point energy and therefore should have the largest population.

We have applied the same formalism to Rb^*He_n exciplexes. The energetic structure of Rb^*He_n exciplexes is quite different from Cs^*He_n, as the zero point energies of Rb^*He_n for $n = 1$ to $n_{max} = 6$ are well below the dissociation limit and all corresponding exciplexes are stable. Therefore rubidium, in contrast to cesium, has no activation barrier for the sequential formation of the $Rb^*He_{n>2}$ exciplexes, which was convincingly evidenced by the observation [4] of population in all Rb^*He_n complexes with n = 1...6. The results of our simplified treatment of the molecular vibrations for both Cs^*He_n and Rb^*He_n exciplexes are in very good agreement with more sophisticated Hartree-Fock and *ab initio* calculations [3, 4].

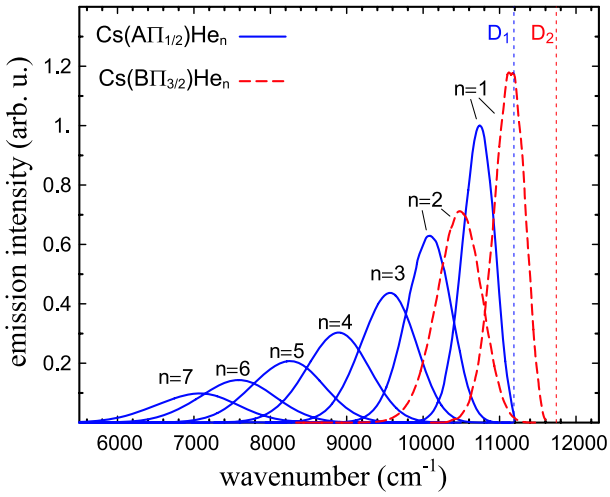

FIG. 6: Calculated emission lines of the $Cs(A\Pi_{1/2})He_n$ exciplexes for $n = 1$ to $n = 7$ (solid curves) and of $Cs(B\Pi_{3/2})He_n$ exciplexes for $n = 1, 2$ (dashed curves). The lines are red-shifted and become broader with increasing number of helium atoms n. The dashed vertical lines indicate the positions of the free atomic D_1 and D_2 emission lines.

C. The emission spectra

We calculate the emission spectra $I(\nu)$ of the different exciplexes in the Franck-Condon approximation by

$$I(\nu) \propto \nu^3 \left| \int \Psi(r,\nu)\Psi_{sym}(r)dr \right|^2, \qquad (12)$$

where ν is the transition frequency and $\Psi(r,\nu)$ is the wave function of the Cs^*He_n configuration in the electronic ground state $X\Sigma_{1/2}$. Because of the radial symmetry of $\Psi(r,\nu)$ the integrals over the angular variables do not influence the shape of the emission lines. As mentioned above we consider only the wave function $\Psi_{sym}(r)$ of the breathing mode oscillation in the excited state of the exciplex.

Fig. 6 shows the calculated emission lines from the vibrational ground states of the $Cs(A\Pi_{1/2})He_{n=1...7}$ and $Cs(B\Pi_{3/2})He_{n=1,2}$ exciplexes. The red shift of the lines with increasing n is mainly due to the steep repulsive potential of the ground state potential $nV_\sigma^{6s}(r)+V_n^{He\text{-}He}(r)$, and the corresponding broadening is due to the increase of the slope of that potential. The integral intensity of the lines drops with decreasing frequency ν, mainly because of the ν^3-dependence in (12). The asymmetry of the lines originates from the asymmetric shape of the excited state wavefunction $\Psi_{sym}(r)$ and from the curvature of the ground state potential.

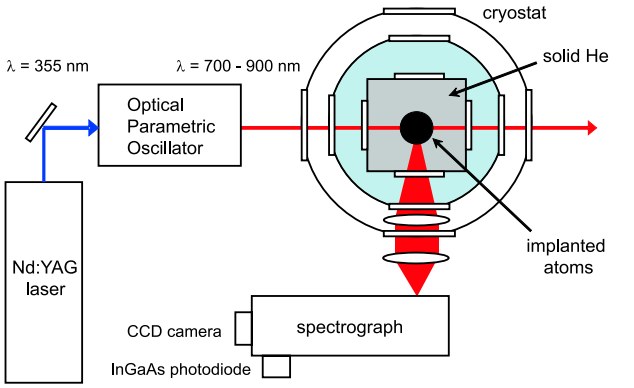

FIG. 7: Top view of the helium containment part of the cryostat (cross-section, not to scale) and setup for laser-induced fluorescence measurements.

III. EXPERIMENT

A. Experimental setup

The experimental setup is illustrated in Fig. 7. A ^{4}He matrix doped with Cs atoms was produced by the technique described in our earlier papers [14–16]. Data were taken in the hcp and bcc phases of solid ^{4}He at a temperature of 1.5 K and in a pressure range of $27 - 36$ bar. The experiments were performed in a helium pressure cell immersed in superfluid helium cooled by pumping on the helium bath. Windows provide optical access from three orthogonal directions. A helium crystal is grown inside the pressure cell, by first condensing helium gas from an external reservoir and then raising the pressure on the gas supply line. The helium host matrix is doped with cesium atoms by means of laser ablation with a pulsed frequency-doubled Nd:YAG-laser beam focused onto a solid Cs target by a height-adjustable lens above the cell.

The cesium atoms implanted into the helium crystal are excited by radiation from an optical parametric oscillator (OPO), (OPTA GmbH, BBO-355-vis/IR) pumped by the third harmonic (354 nm) of a Nd:YAG laser. The latter is pulsed with a repetition rate of 10 Hz. We used the idler beam of the OPO, whose wavelength can be tuned over the range of 800 nm - 2.4 μm. The OPO beam is horizontally polarized and the direction of observation is along the light polarization, thereby minimizing the background from non-resonant scattered light. The average light power at the entrance of the cryostat is controlled by means of a $\lambda/2$ plate and a polarizer. During the experiment it was kept at the level of 1 mW in order to prevent melting of the He crystal.

The atomic fluorescence light from the sample volume (approx. 3 mm^3) is collimated by a lens in the cryostat and then focused into a grating spectrograph (Oriel, MS257) with a resolution of 20 cm^{-1}. Depending on the spectral domain two different photodetectors are used. Visible and near infrared fluorescence is detected by means of a CCD camera attached to the spectrograph,

while for the wavelengths above 1 μm an InGaAs photodiode is used. In the latter case the grating is rotated by a step-motor and spectra are recorded point by point.

B. Observed emission spectra

In the experiments the wavelength of the excitation laser is scanned over either the $6S_{1/2}$-$6P_{1/2}$ (D_1 transition) or the $6S_{1/2}$-$6P_{3/2}$ (D_2 transition) line, which are the transitions to the lowest lying excited states of the Cs atom. Both atomic lines are broadened and blue shifted due to the interaction with the helium matrix. The shift and broadening of both absorption lines were studied earlier [2, 17] and are well understood in the frame of the bubble model, which is valid both for liquid and solid helium matrices. Fig. 8(a) represents a typical emission spectrum following D_1 excitation at 11760 cm^{-1} (850 nm). The rightmost peak in the spectrum (labelled **e**) is due to the laser light scattered into the spectrograph. The atomic cesium emission from the pumped transition appears at 11360 cm^{-1} (880 nm) as the line **a** in Fig. 8(a). The amplitude of that peak does not represent its real value because of detector saturation. The large Stokes shift of 400 cm^{-1} between the excitation and emission wavelengths for transitions between the same two atomic states is a typical feature of the atomic bubbles: the excitation takes place in a small bubble formed by the cesium atom in its ground state, while the emission occurs in a larger bubble corresponding to the larger size of the excited state. The interaction with the smaller bubble shifts the atomic line more than the interaction with the larger bubble, which explains the Stokes shift.

A very weak and broad emission line is centered at 10200 cm^{-1} (line **c** in Fig. 8(a)). It is attributed to the bound-free quasi molecular transition of a Cs($A\Pi_{1/2}$)He_2 exciplex (see Fig. 8(c)). The corresponding calculated spectrum (scaled in amplitude) is shown in Fig. 8(a) as a solid line, which shows a remarkable agreement with the experimental curve. Another exciplex emission line appears further to the red (line **d** in Fig. 8(a)) around 7200 cm^{-1}. This line is believed to originate from higher order ($n > 2$) dumbbell-shaped exciplexes. For this peak the best agreement between measured and calculated spectra is achieved for two species: Cs($A\Pi_{1/2}$)He_6 and Cs($A\Pi_{1/2}$)He_7. The corresponding calculated curves are shown in Fig. 8(a).

The emission spectrum following D_2 excitation at 12500 cm^{-1} (800 nm) is shown in Fig. 8(b). Its structure is very similar to the one discussed above (scattered laser light not shown). No fluorescence corresponding to the D_2 transition is detected. However, a weak fluorescence (line **a**) at 11360 cm^{-1}, corresponding to D_1 emission is observed. This indicates the existence of a fine-structure relaxation channel. The first exciplex emission (line **b**) appears at 10520 cm^{-1}, and does not coincide with the feature **c** in Fig. 8(a). We attribute this peak to emission by a Cs($B\Pi_{3/2}$)He_2 exciplex (see Fig. 8(c)), which was previously observed in liquid helium and in cold helium gas by the group in Kyoto [3]. The calculated spectrum of this molecule is in a good agreement with the experiment as shown by the solid line in Fig. 8(b). The strongest emission line at 7200 cm^{-1} belongs to the same molecule as the feature **d** in Fig. 8(a): either Cs($A\Pi_{1/2}$)He_6, or Cs($A\Pi_{1/2}$)He_7.

C. Excitation spectra

So far we have discussed the fluorescence spectra induced by absorption of light of a fixed (resonant) frequency. We now address the excitation spectra, i.e., the dependence of the emitted fluorescence in the different channels on the wavelength of the exciting laser. The results are shown in Fig. 9. One distinguishes two distinct regions of resonant absorption, centered at 11800 cm^{-1} (847 nm) and 12500 cm^{-1} (800 nm). These regions can be identified with excitation to the atomic $6P_{1/2}$ and $6P_{3/2}$ states of Cs, which we refer to as D_1 and D_2 absorption lines. For each scan of the excitation wavelength the fluorescence detecting spectrometer was adjusted to the peak of one of the emission lines of Fig. 8. The labelling $(a)\ldots(d)$ in Fig. 9 corresponds to the labelling of the corresponding fluorescence channels in Fig. 8.

Fig. 9(a) shows that atomic fluorescence via the D_1 channel can be induced both by D_1 and by D_2 absorption. The D_1 excitation line is slightly asymmetric [2] and has a width of about 200 cm^{-1}. The D_2 excitation line of the same fluorescence has a pronounced double structure that is well fitted by two Gaussians split by approximately 250 cm^{-1}. Fig. 9(b) shows that fluorescence from the Cs($A\Pi_{1/2}$)He_2 exciplex can only be observed after D_1 excitation, whereas the Cs($B\Pi_{3/2}$)He_2 exciplex is formed only after D_2 excitation (Fig. 9(c)). The dumbbell-shaped exciplex Cs($A\Pi_{1/2}$)$He_{n>2}$ can be formed by D_1 or by D_2 absorption (Fig. 9(d)). The emission lines of the exciplexes are about two orders of magnitude stronger in Fig. 8(b) than in Fig. 8(a), while the atomic emission has an opposite behavior with D_1 excitation yielding a 100 times stronger fluorescence than D_2 excitation. In fact, in the experiment with D_2 excitation the emission of the exciplexes is much stronger than the atomic fluorescence.

The double-peaked D_2 excitation spectra were observed before for atomic cesium and rubidium in superfluid helium [18] and for Cs*He and Rb*He exciplexes on superfluid helium nanodroplets [9, 19]. The blue component of the doublet has always a larger spectral width and a smaller amplitude than the red component. In condensed helium the splitting between the two components increases with helium pressure and an extrapolation of the data from [18] to our pressures gives a value of the splitting very close to the one measured here in solid helium. The authors of [18] suggested that the double peak reflects a lifting of the m_J level degeneracy of the $6P_{3/2}$ state induced by quadrupolar bubble shape os-

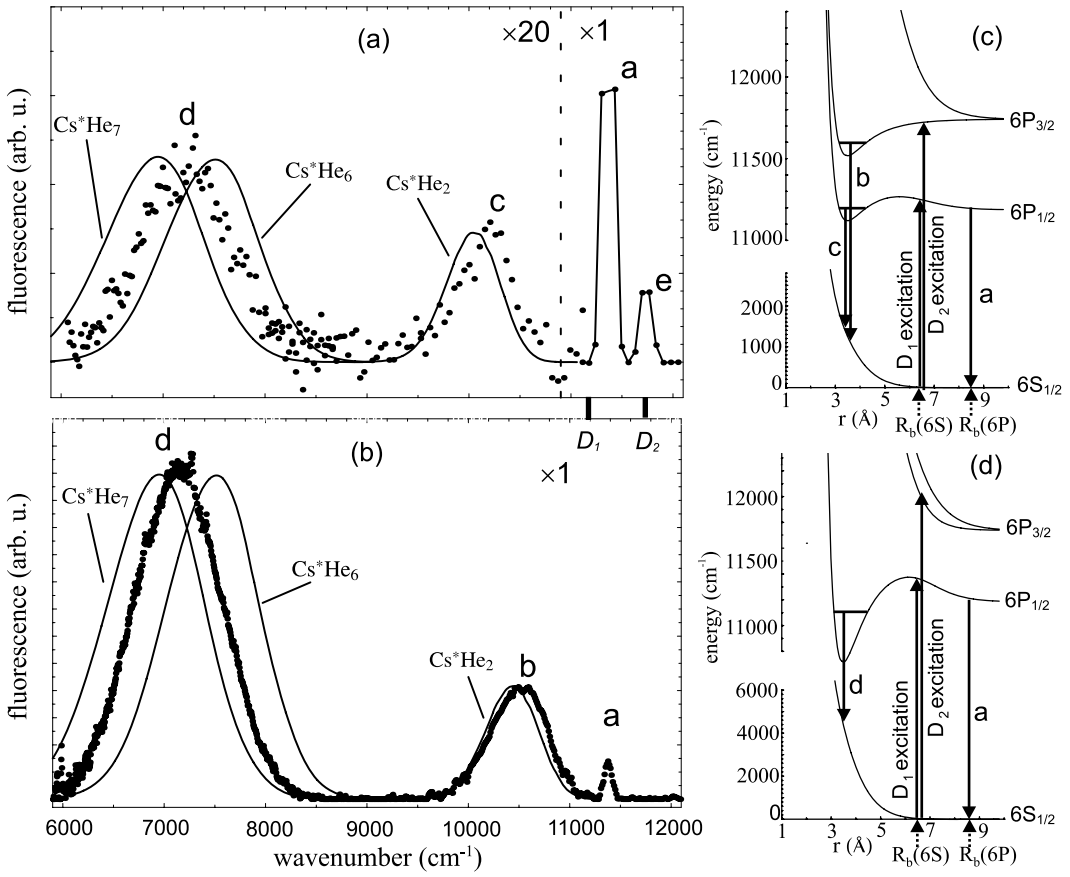

FIG. 8: (a) and (b) - measured emission spectra (dots) of atomic Cs and Cs^*He_n exciplexes at T=1.5 K, p=30 bar in the hcp crystalline phase of ^{4}He. (a) fluorescence following D_1 excitation (11800 cm^{-1}); (b) fluorescence following D_2 excitation (12500 cm^{-1}). The peaks are labelled as follows: **a**- fluorescence of atomic Cs via the D_1 transition; **b**- fluorescence from the apple-shaped $Cs(B\Pi_{3/2})He_2$ exciplex; **c**- Fluorescence from the apple-shaped $Cs(A\Pi_{1/2})He_2$ exciplex; **d**- fluorescence from the dumbbell-shaped $Cs(A\Pi_{1/2})He_{n>2}$ exciplex; **e**- scattered laser light. The corresponding calculated spectra are shown as continuous lines with scaled amplitudes for each line. Note the rescaling by a factor 20 of the lines **c** and **d** in (a) with respect to the lines **a** and **e**. Vertical bars show the position of the D_1 and D_2 transition in the free Cs atom. (c) and (d) - potential energy diagrams of Cs^*He_2 and Cs^*He_7. The solid vertical arrows indicate absorption and emission (labelling corresponds to that of (a) and (b)). The dotted arrows mark the equilibrium values of the bubble radius in the 6S and $6P_{1/2}$ states.

cillations. However, the calculated line splitting based on that assumption yields a splitting, which is approximately two times smaller than the measured one [18]. On the other hand, similar results were obtained by numerical simulations using path-integral Monte Carlo [20] and density-functional techniques [21]. In all cases the splitting appears to be due to an anisotropic instantaneous distribution of He atoms around the impurity.

D. Pressure shift of the exciplex emission lines

We have measured the dependence of the emission line centers as a function of helium pressure. The wavelength of the excitation laser was tuned to 12500 cm^{-1} (D_2 excitation), the temperature was kept constant at 1.5 K, and the pressure of helium scanned slowly in the range of 27-36 bar, covering both the bcc and the hcp phases of the helium matrix. The positions of the emission peaks were inferred by calculating their centers of gravity. The results are shown in Fig. 10.

Fig. 10(a) shows the position of the atomic D_1 emission line (peak **a** in Fig. 8(b)) measured by using the CCD camera on the spectrograph. The line is blue shifted with respect to the free atomic transition and the shift increases with helium pressure. The steep increase of the emission wave number at about 27.5 bar by about 20 cm^{-1} marks the phase transition from the bcc crystalline phase of helium to the hcp phase.

The pressure shift of the $Cs(B\Pi_{3/2})He_2$ emission peak (peak **b** in Fig. 8(b)) was measured with the same detection system. As can be seen in Fig. 10(b) it shifts in a similar manner than the atomic fluorescence. However, the slope of the pressure shift and the jump at the phase transition are significantly larger for the exciplex.

Fig. 10(c) shows the pressure dependence of the

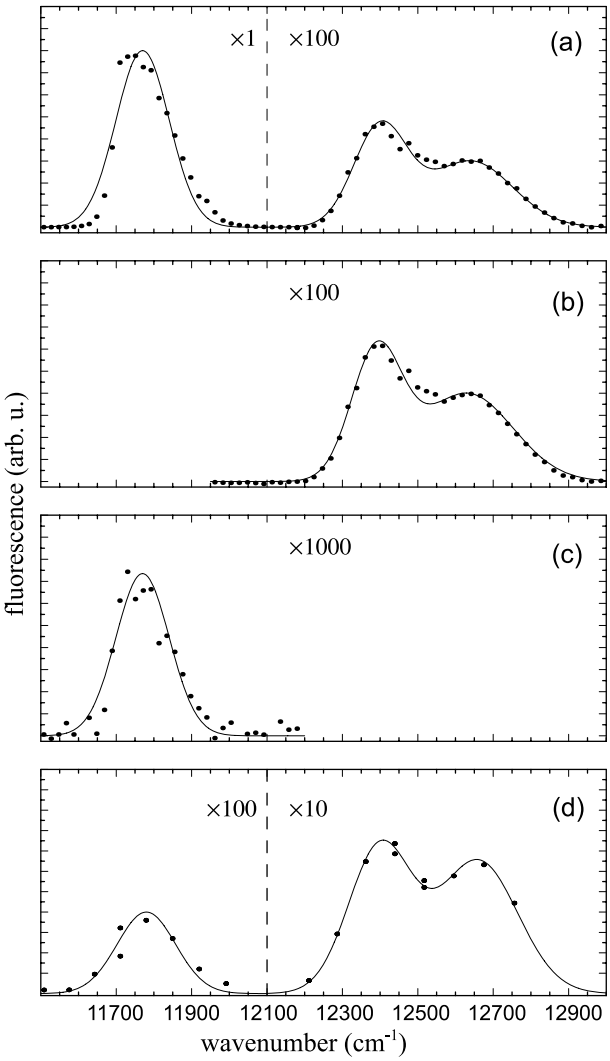

FIG. 9: Measured excitation spectra of atomic Cs and Cs^*He_n exciplexes (dots): (a) atomic Cs $6P_{1/2}$ state; (b) apple-shaped $Cs(B\Pi_{3/2})He_2$ exciplex; (c) apple-shaped $Cs(A\Pi_{1/2})He_2$ exciplex; (d) dumbbell-shaped $Cs(A\Pi_{1/2})He_{n>2}$ exciplex. The D_1 excitation line is centered at 11800 cm^{-1}, and the D_2 excitation line has a double-peak structure centered at 12500 cm^{-1}. The continuous line is a fit made by three gaussians. Data in (a)-(c) measured by the CCD camera, (d) - by InGaAs photodiode.

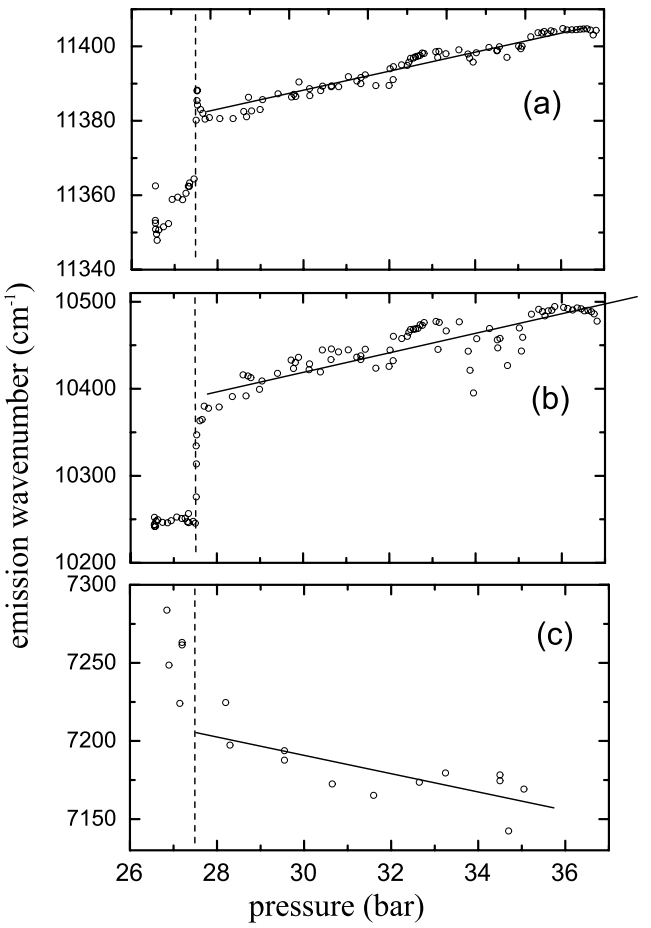

FIG. 10: Pressure dependence of atomic and exciplex emission lines measured at 1.5 K, under D_2 excitation: (a) atomic D_1 fluorescence, (b) $Cs(B\Pi_{3/2})He_2$ exciplex emission, (c) $Cs(A\Pi_{1/2})He_{n>2}$ exciplex emission. The dashed line indicates the phase boundary between the b.c.c. and the h.c.p. crystalline phases of solid ^{4}He. The solid lines are linear fits to the data points in the h.c.p. phase.

$Cs(A\Pi_{1/2})He_{n>2}$ emission peak. The spectra were taken point by point using the InGaAs photodiode as detector in the spectrograph. In contrast to $Cs(B\Pi_{3/2})He_2$, the emission line of the dumbbell-shaped exciplex with increasing pressure shifts to the red. The value of the slope (but not its sign) of the pressure shift changes at the phase transition between the bcc and the hcp phases. It should be noted that in the bcc phase the exciplex emission is much weaker than in the hcp phase. The same effect is observed for the atomic fluorescence and is believed to be the consequence of alkali clusters formation. As the molar density of helium in the bcc phase is lower than in the hcp phase, the crystal becomes softer and allows for the motion of Cs atoms towards each other and the formation of molecules and large clusters. This reduces the density of available Cs atoms and hence the formation rate of Cs^*He_n exciplexes.

An alternative, speculative interpretation of this behavior may be due to bubble deformations. From previous studies [22] it is known that the atomic ground state bubbles have a quadrupolar deformation on the order of 5%. As the hcp matrix is most probably polycrystalline the axes of these deformed bubbles are randomly oriented. The exciplexes observed here are also strongly anisotropic. Although the orientation of the exciplex symmetry axis is determined by the orientation of the (linear) laser polarization, the exciplex may reorient itself along the axis of the deformed bubble in order to minimize its energy. A future analysis of the fluorescence polarization might shine more light on this. In a configuration, in which the bubble and exciplex axes are aligned

the helium atoms on the bubble surface may be closer to the nodal line/plane, which would favor the exciplex formation compared to the configuration with spherical bubbles in the bcc phase.

In the model calculations discussed in Sec. II we have considered only the cesium atoms together with the helium atoms that form the exciplex and have neglected the influence of the helium atoms from the bubble surface and the helium bulk. In that sense the helium pressure is not a parameter in our model. The fact that we observe a pressure dependence clearly shows the limits of our model assumptions. However, the maximum shifts observed in the investigated range of pressures are only a small fraction of the width of the exciplex emission lines, so that the disregard of the bulk is justified, when aiming at an agreement at the level of the linewidth. Calculations taking bubble contributions into account are currently in progress.

IV. DISCUSSION

A. Assignment of the observed emission peaks

The theoretical model presented in Sec. II has allowed us to calculate the emission spectra of different Cs^*He_n exciplexes, which are in good agreement with the experimental results (Fig. 8). The best agreement for the peak near 10000 cm^{-1} is achieved for the Cs^*He_2 complex. Two different electronic states of this molecule are populated by D_1 and D_2 pumping. According to Fig. 3 the $B\Pi_{3/2}$ state originates from the $6P_{3/2}$ state of the free cesium atom and may be populated only by absorption via the D_2 atomic transition. The corresponding calculated emission peak is centered at 10500 cm^{-1}, in excellent agreement with the experiment. The $A\Pi_{1/2}$ state is related to the $6P_{1/2}$ atomic state and can be populated by the D_1 pumping. The calculated emission line is at 10200 cm^{-1}, in agreement with the measurements. The $Cs(B\Pi_{3/2})He_2$ exciplex (peak **b** in Fig. 8(b)) has been observed before in liquid [3] and in solid helium [10]. To our knowledge the observation of the $Cs(A\Pi_{1/2})He_2$ state shown as peak **c** in Fig. 8(a) is reported here for the first time.

The correct assignment of the measured peak at 7200 cm^{-1} in Fig. 8 is a more subtle task. It is clear that the line originates from a $Cs(A\Pi_{1/2})He_{n>2}$ exciplex, in which the helium atoms form a ring in the nodal plane of the Cs valence electron distribution. As the ring-shaped exciplexes contain a larger number of helium atoms any imprecision of the initial pair potentials will increase with the number of He atoms involved. As a consequence the positions of the $Cs^*He_{n>2}$ emission peaks will be predicted with less accuracy than the one of Cs^*He_2. One sees that the calculated spectra of Cs^*He_6 and Cs^*He_7 give a reasonable overlap with the measured peak. The overall good agreement between calculated and measured lineshapes (in particular the width) indicates that the line at 7200 cm^{-1} originates from the decay of an exciplex with a specific number $n = n_{max}$ of bound helium atoms and that it is not a superposition of lines from exciplexes with different values of n. Such superpositions were observed in the case of Rb^*He_n exciplexes in cold ^{4}He vapor [4] as a consequence of the sequential formation process.

The identification of the peak **d** in Fig. 8 is ambiguous. At first sight the calculated spectra of both Cs^*He_6 and Cs^*He_7 fit the observed line equally well. However, as mentioned above, our theoretical model does not take the interaction between the exciplex and the surrounding helium matrix into account. Therefore, the calculated peaks positions should be considered as asymptotic values at zero helium pressure. The experimental pressure dependence (Fig. 10 (c)) of the peak **d** from Fig. 8(b) shows that it shifts to the blue when going to lower pressure, thereby bringing the calculated line of Cs^*He_6 into better agreement with the experimental data. On the other hand the calculated zero-point energies of the exciplexes (Fig. 5) show that the complex with 7 bound helium atoms is the largest stable dumbbell-shaped exciplex, which would support Cs^*He_7 to be at the origin of the observed fluorescence.

B. Formation of the Cs^*He_2 exciplex

According to the bubble model [2, 17] Cs atoms in solid helium reside in small cavities, the so-called atomic bubbles. The bubbles result from the equilibrium of the surface tension and the pressure-volume energy on one hand and the repulsive force between the alkali valence electron and the closed S shell electrons of helium (Pauli principle) on the other hand. Therefore, the size and shape of the atomic bubble are determined by the size and symmetry of the valence electron density of the impurity atom. As a consequence the bubble formed by a ground state Cs atom in bcc He is spherical with a radius $R_b(6S)\approx 6.5$ Å, as is indicated in Fig. 8(c) and (d) by dotted arrows. According to the Franck-Condon approximation, R_b does not change during the excitation process to the 6P states. After the atomic excitation the bubble relaxes by increasing its radius to $R_b(6P)\approx 8.5$ Å in order to accommodate the larger size of the excited state. Helium atoms located near the intersection points of the quantization axis (determined by the laser polarization) with the bubble surface experience an attractive potential. They will hence approach the Cs atom and form a linear triatomic molecule with an equilibrium interatomic distance of 3.5 Å. The bound state configuration is labelled $B\Pi_{3/2}$ in Fig. 3. Due to the large density of nearby helium atoms only $Cs(B\Pi_{3/2})He_2$ will be formed as the two possible binding centers will be filled quasi instantaneously. This is in contrast with the observations of the same exciplex in cold helium gas, where, due to the much smaller collision rate the binding sites are filled in a sequential order, as evidenced by the observation

of fluorescence from Cs($B\Pi_{3/2}$)He$_1$ and Cs($B\Pi_{3/2}$)He$_2$ exciplexes [3].

The formation mechanism of Cs($A\Pi_{1/2}$)He$_2$ exciplex following the excitation of the $6P_{1/2}$ atomic state (D_1 transition) is more complex. There is a potential barrier of 19 cm^{-1} in the $A\Pi_{1/2}$ state with respect to $V_{Cs^*He_n}(r = R_b(6S))$ located at r = 6.1 Å(see Fig. 3), inside the bubble. In order to form a molecule, one or two helium atoms have to tunnel through this barrier. Therefore the formation of Cs*He$_2$ exciplexes under D_1 pumping is much less efficient, the main decay channel from the $6P_{1/2}$ state being via the strong D_1 emission line (feature **a** in Fig. 8(a)).

When the energy of the pair of He atoms is close to that of a ro-vibrational eigenstate of the exciplex, the tunnelling probability will be resonantly enhanced. Immediately after the excitation of the Cs atom the separation to the nearest helium atoms is $R_b(6S)$, and their energy can be approximated by the value of the potential energy of the exciplex at this distance. As the bubble expands, the energy decreases and passes through one or several such resonances. Our calculations suggest the formation of Cs($A\Pi_{1/2}$)He$_2$ is mainly due to a resonance with the vibration state v=2, located 44 cm^{-1} above the atomic $6P_{1/2}$ state) at R_b = 6.95 Å. At exact resonance the tunnelling probability, i.e. the probability of crossing the barrier at each attempt made by the He atoms, is close to unity. Following the approach of [8], the frequency of such attempts can be assumed to be on the order of the Debye frequency of solid helium. According to [23] the Debye temperature in the hcp phase at 1.5 K and 30 bar is 24 K, and the resulting tunnelling time is approximately 2 ps. The speed of the bubble expansion, i.e. of the formation of an atomic $P_{1/2}$ state may be estimated as the sound velocity V_s=220-250 m/s in the hcp phase [24]. The resulting probability to form the exciplex relative to the population of the atomic state is on the order of 10^{-4}. However, a recent study of the dynamics of He_2^* exciplex bubbles in superfluid helium [25] have shown that the expansion speed is much smaller than the speed of sound and does not exceed 20 m/s. With the latter value we obtain a probability for exciplex formation on the order of 10^{-3}, which agrees well with the measured ratio of integrated exciplex and atomic Cs fluorescence intensities.

C. Formation of the Cs*He$_{n_{max}}$ exciplex

Fig. 4 shows that the $A\Pi_{1/2}$ state of the Cs*He$_7$ complex originates from the $|6P_{1/2}, m_J = \pm 1/2\rangle$ atomic states. Its formation process upon the D_1 excitation is similar to that of Cs($A\Pi_{1/2}$)He$_2$; it proceeds via tunnelling through the potential barrier. As the excitation takes place at the equilibrium radius of the ground state $r = R_b(6S)$=6.5 Å, the Franck-Condon transition excites the $A\Pi_{1/2}$ configuration near the maximum of the potential barrier.

We recall that the potential energy diagram in Fig. 4 was calculated by assuming that all 7 helium atoms move towards the Cs atom simultaneously. This happens via the collective breathing mode of the bubble oscillations. Under the assumption that all 7 helium atoms make the tunnelling transition simultaneously, the formation of the exciplex is due to a resonance with a vibration state near v=16, which lies 160 cm^{-1} above the atomic $6P_{1/2}$ state at R_b = 6.8 Å. Using the same approach as above the tunnelling probability for Cs($A\Pi_{1/2}$)He$_2$ formation is on the order of $6{\cdot}10^{-4}$, which is approximately two times less than the ratio of measured intensities. The agreement is quite satisfactory, when considering the approximations made. There are other formation processes, which proceed via two steps. We recall that the potential barrier is associated with a structural change of the $6P_{1/2}$ wave function from spherical to dumbbell-shaped. If three, or more He atoms tunnel through the barrier and form a bound state, the dumbbell shape is formed and the barrier disappears. In a second step more He atoms can be captured until they fill the available space around the waist of the dumb-bell. Such processes, in which less than n_{max} atoms are captured in the first step may be initiated by asymmetric oscillation modes of the bubble.

The excitation of the Cs atom to the $6P_{3/2}$ state (D_2 transition) represents another, much more efficient mechanism for the formation of Cs($A\Pi_{1/2}$)He$_{n_{max}}$. It involves a mixing of the fine-structure components. In fact, both $6P_{3/2}$ and $6P_{1/2}$ atomic states are coupled by the interaction with the helium ring and the resulting $A\Pi_{1/2}$ and $B\Pi_{3/2}$ molecular states are r-dependent mixtures of the asymptotic $|P_{3/2},\ m_j = \pm 1/2\rangle$ and $|P_{1/2},\ m_j = \pm 1/2\rangle$ states

$$|A\Pi_{1/2}\rangle = a(r)|P_{1/2}, \pm 1/2\rangle + b(r)|P_{3/2}, \pm 1/2\rangle \quad (13)$$
$$|B\Pi_{3/2}\rangle = b(r)|P_{1/2}, \pm 1/2\rangle - a(r)|P_{3/2}, \pm 1/2\rangle \quad (14)$$

The r-dependencies of the mixing probabilities $|a|^2$ and $|b|^2$ are shown in Fig.11(b). The coupling of the $A\Pi_{1/2}$ and $B\Pi_{3/2}$ states leads to an avoided crossing of the two potential curves at $r \simeq 6$ Å. At smaller interatomic distances the $A\Pi_{1/2}$ state correlates mostly to the $6P_{3/2}$, while $B\Pi_{3/2}$ correlates to $6P_{1/2}$. The avoided crossing is illustrated in Fig. 11(a), where bold lines represent adiabatic molecular potentials identical to that of Fig. 4, while broken lines show the diabatic potentials when the coupling between molecular states is neglected. The diabatic potentials are constructed using the same model as described in Sec. II, where, instead of the diagonalization of the general expression (4) for the molecular Hamiltonian, the spin-orbit term is diagonalized separately and then added to the interatomic interaction. The excitation takes place at $r = R_b(6S)$ very close to the anticrossing point, where the probability of a radiationless transition $B\Pi_{3/2} \rightarrow A\Pi_{1/2}$ is high. This results in a very fast formation of the Cs($A\Pi_{1/2}$)He$_{n_{max}}$ exciplex and provides a density much higher than those of Cs($A\Pi_{1/2}$)He$_2$ and

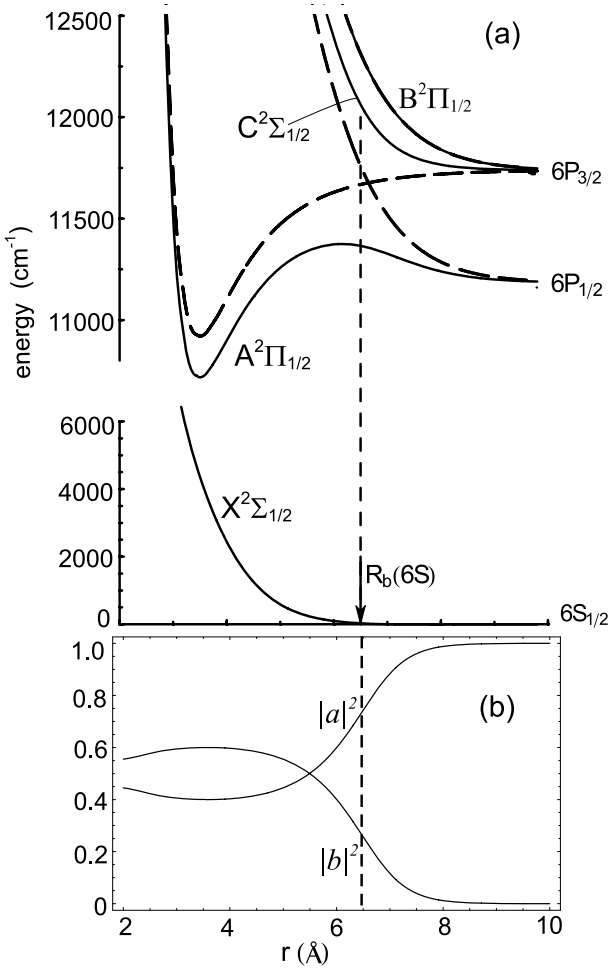

FIG. 11: (a) The potential energy diagram of Cs^*He_7: bold lines - adiabatic potentials, broken lines - diabatic potentials (see the text). Vertical broken line shows the interatomic separation at which the excitation takes place. (b) The r-dependence of the probability $|a|^2$ that $A\Pi_{1/2}$ state of Cs^*He_7 is in the $|P_{1/2}, \pm 1/2\rangle$ state and the probability $|b|^2$ to be in the $|P_{3/2}, \pm 1/2\rangle$ state.

atomic $Cs(6P_{1/2})$, as is evidenced by the relative integral fluorescence intensities in Fig.8(b).

V. SUMMARY

We have performed a study of laser induced fluorescence of cesium atoms trapped in the hcp and bcc phases of a helium crystal. The spectral range of both absorption and emission wavelengths was significantly enlarged with respect to previous studies. In addition to the well-studied atomic fluorescence following D_1 excitation we observed a number of new spectral features. We have found for the first time a weak emission of atomic D_1 fluorescence following excitation on the D_2 line. As observed before in superfluid helium the corresponding absorption line has a double-peaked structure. In addition we have discovered three spectral features, which are broader and in some cases much more intense than the atomic lines. We have shown that these lines are formed by the emission from two types of specific Cs^*He_n exciplex structures, viz. an apple-shaped complex with two helium atoms bound to the Cs atom and a dumbbell-shaped complex, in which a ring of helium atoms is bound to the nodal plane of the Cs wave function. These assignments were based on model calculations, which have allowed us to calculate the positions and shapes of the corresponding emission lines. In the case of the ring structure the number of bound atoms cannot be determined unambiguously, but the calculations suggest $n = 6$ or $n = 7$ to be the most likely number of bound atoms. The theoretical treatment is approximative in the sense that it considers only the bound He atoms, while neglecting the effect of nearby atoms of the surrounding helium matrix. Ongoing work is supposed to shine more light on this problem, by including spherical and deformed bubbles into the calculation.

Acknowledgments

We like to thank J. Pascale for sending us his numerical Cs-He pair potentials. This work was supported by the grant number 200020-103864 of the Schweizerischer Nationalfonds.

[1] J. Dupont-Roc, Z. Phys. B **98**, 383 (1995).
[2] S. Kanorsky, A. Weis, M. Arndt, R. Dziewior, and T. W. Hänsch, Z. Phys. B **98**, 371 (1995).
[3] K. Enomoto, K. Hirano, M. Kumakura, Y. Takahashi, and T. Yabuzaki, Phys. Rev. A **66**, 042505 (2002).
[4] K. Hirano, K. Enomoto, M. Kumakura, Y. Takahashi, and T. Yabuzaki, Phys. Rev. A **68**, 012722 (2003).
[5] K. Enomoto, K. Hirano, M. Kumakura, Y. Takahashi, and T. Yabuzaki, Phys. Rev. A **69**, 012501 (2004).
[6] C. Schulz, P. Claas, and F. Stienkemeier, Phys. Rev. Lett. **87**, 153401 (2001).
[7] J. Reho, J. Higgins, C. Callegari, K. K. Lehmann, and G. Scoles, J. Chem. Phys. **113**, 9686 (2000).
[8] J. Reho, J. Higgins, K. K. Lehmann, and G. Scoles, J. Chem. Phys. **113**, 9694 (2000).
[9] F. R. Bruhl, R. A. Trasca, and W. E. Ernst, J. Chem. Phys. **115**, 10220 (2001).
[10] D. Nettels, A. Hofer, P. Moroshkin, R. Müller-Siebert, S. Ulzega, and A. Weis, Phys. Rev. Lett. **94**, 063001 (2005).
[11] J. Pascale, Phys. Rev. A **28**, 632 (1983).
[12] R. A. Aziz and A. R. Janzen, Phys. Rev. Lett. **74**, 1586 (1995).
[13] P. Gombás, *Pseudopotentiale* (Springer-Verlag - Wien -

New York, 1967).
[14] M. Arndt, R. Dziewior, S. Kanorsky, A. Weis, and T. W. Hänsch, Z. Phys. B **98**, 377 (1995).
[15] S. Kanorsky, M. Arndt, R. Dziewior, A. Weis, and T. W. Hänsch, Phys. Rev. B **49**, 3645 (1994).
[16] D. Nettels, R. Müller-Siebert, S. Ulzega, and A. Weis, Applied Physics B **77**, 563 (2003).
[17] T. Kinoshita, K. Fukuda, Y. Takahashi, and T. Yabuzaki, Phys. Rev. A **52**, 2707 (1995).
[18] T. Kinoshita, K. Fukuda, and T. Yabuzaki, Phys. Rev. B **54**, 6600 (1996).
[19] O. Bunermann, M. Mudrich, M. Weidemuller, and F. Stienkemeier, J. Chem. Phys. **121**, 8880 (2004).
[20] S. Ogata, J. Phys. Soc. Jpn. **68**, 2153 (1999).
[21] T. Nakatsukasa, K. Yabana, and G. F. Bertsch, Phys. Rev. A **65**, 032512 (2002).
[22] S. Kanorsky, S. Lang, T. Eichler, K. Winkler, and A. Weis, Phys. Rev. Lett. **81**, 401 (1998).
[23] G. Ahlers, Phys. Rev. **135**, 10 (1964).
[24] R. H. Crepeau, O. Heybey, D. M. Lee, and S. A. Strauss, Phys. Rev. A **3**, 1162 (1971).
[25] A. V. Benderskii, J. Eloranta, R. Zadoyan, and V. A. Apkarian, J. Chem. Phys. **117**, 1201 (2002).